Differential contribution of the NR1- and NR2A-subunits to the selectivity filter of recombinant NMDA receptor channels

Lonnie P. Wollmuth, Thomas Kuner*, Peter H. Seeburg* and Bert Sakmann

*Max-Planck-Institut für medizinische Forschung, Abteilung Zellphysiologie, Jahnstrasse 29, D-69028 Heidelberg and *Center for Molecular Biology (ZMBH), Heidelberg University, Im Neuenheimer Feld 282, D-69120 Heidelberg, Germany*

1. The molecular determinants for the narrow constriction of recombinant *N*-methyl-D-aspartate (NMDA) receptor channels composed of wild-type and mutant NR1- and NR2A-subunits were studied in *Xenopus* oocytes.

2. The relative permeability of differently sized organic cations was used as an indicator of the size of the narrow constriction. From measured reversal potentials under bi-ionic conditions with K^+ as the reference solution, permeability ratios were calculated with the Lewis equation.

3. For wild-type NMDA receptor channels, five organic cations showed clear reversal potentials, with permeability ratios (P_X/P_K): ammonium, 1·28; methylammonium, 0·48; dimethylammonium (DMA), 0·20; diethylammonium, 0·07; and dimethylethanol-ammonium, 0·02.

4. Mutation of the N-site asparagine (N) to glutamine (Q) at homologous positions in either NR1 (position 598) or NR2A (position 595) increased the permeability of DMA relative to wild-type channels about equally. However, for larger sized organic cations, the NR1(N598Q) mutation had stronger effects on increasing their permeability whereas the NR2A(N595Q) mutation was without effect. These changes in organic cation permeability suggest that the NR1(N598Q) mutation increases the pore size while the NR2A(N595Q) mutation does not.

5. Channels in which the NR1 N-site asparagine was replaced by the smaller glycine (G), NR1(N598G)–NR2A, showed the largest increase in pore size of all sites examined in either subunit. In contrast, in the NR2A-subunit the same N-site substitution to glycine produced only small effects on pore size.

6. For the NR2A-subunit, an asparagine residue (position 596) on the *C*-terminal side of the N-site, when mutated to larger or smaller sized amino acids, produced large, volume-specific effects on pore size. The mutant channel NR1–NR2A(N596G) had the largest increase in pore size of all sites examined in the NR2A-subunit. In contrast, mutation of the homologous position in the NR1-subunit had no effect on pore size.

7. The cross-sectional diameter of the narrow constriction in wild-type NMDA receptor channels was estimated to be 0·55 nm. The pore sizes of the NR1(N598G)–NR2A and NR1–NR2A(N596G) mutant channels increased to approximately 0·75 and 0·67 nm, respectively. The double mutation, NR1(N598G)–NR2A(596G), increased the pore size to approximately 0·87 nm, essentially the sum of the increase produced by the individual mutations.

8. It is concluded that both the NR1- and NR2A-subunits contribute to the narrow constriction of NMDA receptor channels with asparagines located at non-homologous positions. The major determinants of the narrow constriction in NMDA receptor channels are the NR1 N-site asparagine and an asparagine adjacent to the NR2A N-site.

The *N*-methyl-D-aspartate (NMDA) glutamate receptor is a ligand-gated ion channel with a ubiquitous distribution in the vertebrate central nervous system and has been implicated in the molecular mechanism for changes in synaptic efficacy, development of cellular connections and cell death (Cotman & Monaghan, 1988; Choi, 1988; Meldrum & Garthwaite, 1990; Gasic & Hollmann, 1992). The broad physiological role of the NMDA receptor arises in part because its channel is more selective for Ca^{2+} than for monovalent cations and is blocked by external Mg^{2+} in a strongly voltage-dependent manner (Mayer, Westbrook & Guthrie, 1984; Nowak, Bregestovsky, Ascher, Herbet & Prochiantz, 1984; MacDermott, Mayer, Westbrook, Smith & Barker, 1986). Indeed, the Ca^{2+} influx appears to mediate many of the biological functions of NMDA receptor activation (Mayer & Miller, 1988; Cotman & Monaghan, 1988), while the strong voltage-dependent block by Mg^{2+} confers on the NMDA receptor channel a functional dependence of Ca^{2+} influx on membrane potential.

The cDNAs encoding five subunits of the NMDA receptor, one NR1- and four NR2-subunits, have recently been cloned (Moriyoshi, Masu, Ishii, Shigemoto, Mizuno & Nakanishi, 1991; Kutsuwada *et al.* 1992; Monyer *et al.* 1992; Ikeda *et al.* 1992). Native NMDA receptor channels appear to be heteromers composed of NR1- and one or more NR2-subunits (A, B, C, D) (Sheng, Cummings, Roldan, Jan & Jan, 1994). Initially, the NMDA receptor subunits were proposed to share a common membrane topology with other ligand-gated channels which have four proposed transmembrane domains (Hollmann, O'Shea, Rogers & Heinemann, 1989; Kutsuwada *et al.* 1992; Monyer *et al.* 1992). However, subunits of the glutamate family of ligand-gated channels appear to have three membrane-spanning domains (Hollmann, Maron & Heinemann, 1994; Wo & Oswald, 1995; Bennett & Dingledine, 1995). Nevertheless, as in other ligand-gated channels, the M2 domain of both the NR1- and NR2-subunits contributes to the permeation pathway. Based on sequence alignment, an asparagine (N) residue in the M2 domain of both the NR1- and NR2-subunits occupies a site homologous to the Q/R-site in α-amino-3-hydroxy-5-methylisoxazole-4-propionate (AMPA) receptors (Kutsuwada *et al.* 1992; Monyer *et al.* 1992; Hollmann & Heinemann, 1994) and has been termed the N-site (Burnashev, 1993). However, mutation to glutamine of this asparagine residue in the NR1-subunit has strong effects on Ca^{2+} permeation with little effect on Mg^{2+} permeation, whereas the same mutation in the NR2-subunit produces the opposite effect on divalent ion permeation (Burnashev *et al.* 1992). Hence, although the NR1- and NR2-subunits have sequences with a high degree of homology and presumably share a common topology, their M2 domains contribute differently to channel function. The structural basis for this difference is unknown.

Ion channels have a narrow constriction, called the selectivity filter, which acts as a molecular sieve (Hille, 1992). For many ligand-gated channels, this narrow region appears to be a major determinant of ion selectivity (Lester, 1992). As judged by the relative ease by which organic cations of different size permeate the channel, the narrow constriction of recombinant NMDA receptor channels has a cross-sectional diameter of approximately 0·55 nm (Villarroel, Burnashev & Sakmann, 1995), which is smaller than that of other cation-selective ligand-gated channels such as the nicotinic acetylcholine receptor (approximately 0·70–0·74 nm; Dwyer, Adams & Hille, 1980; Wang & Imoto, 1992). In contrast to most other ligand-gated channels, NMDA receptor channels are more selective for Ca^{2+} than for monovalents. In addition, the mechanism of Ca^{2+} permeation in NMDA receptor channels appears to be different from that in voltage-gated Ca^{2+} channels (Zarei & Dani, 1994) where ion binding appears critical (Almers & McCleskey, 1984; Hess & Tsien, 1984). Hence, the smaller dimensions of the NMDA receptor channel may contribute to its divalent ion permeation properties, but the contributions of molecular sieving and ion binding to divalent ion permeation in NMDA receptor channels remain poorly understood.

To identify the structural elements of the permeation pathway of NMDA receptor channels and the amino acids forming the narrow region, we investigated how three consecutive amino acids in the M2 domain of both the NR1- and NR2A-subunits contribute to the narrow constriction. For both subunits, we focused on the N-site as well as two adjacent amino acid residues on the *C*-terminal side of the N-site (Fig. 2*A*); for convenience we refer to these sites as the N + 1 and N + 2 sites. For the NR1-subunit, these residues are serine (N + 1, position S599) and glycine (N + 2, position G600), whereas for the NR2A-subunit they are asparagine (N + 1, position N596) and serine (N + 2, position S597). We systematically changed the volume and charge of the side chain of these amino acids and used the relative ease by which organic cations permeate the channel as an indicator of the size of the narrow constriction.

METHODS

Expression plasmid constructs

Coding regions of the NR1- (R1A splice form; Sugihara, Moriyoshi, Ishii, Masu & Nakanishi, 1992) and the NR2A-subunits (Monyer *et al.* 1992) were cloned into a pSP64T-derived vector optimized for expression in *Xenopus* oocytes (Raditsch *et al.* 1993). Non-coding sequences were stripped and silent restriction sites were introduced to facilitate mutagenesis. The resulting NR1–SP and NR2A–SP clones were used to generate corresponding constructs (NR1–RK, NR2A–RK) in the eukaryotic expression vector pRK (Schall *et al.* 1990) for expression in human embryonic kidney 293 cells (HEK 293). All mutations were introduced in the pSP-based plasmids, and restriction fragments containing mutated positions were cloned into the pRK-based constructs. Amino acids (AA) are shown in the one-letter code. Mutants are named as: subunit(wild-type AA / position in the mature protein / mutant AA).

Site-directed mutagenesis

NR1 subunit. Two silent restriction sites *Nsi*I and *Apa*I flanking the M2 domain were introduced by polymerase chain reaction (PCR)-based methods (Ausubel *et al.* 1994) to allow for insertion of a 72 bp fragment derived from a pair of mutually priming oligonucleotides, one of which contained the mutated nucleotide position. The oligonucleotides were annealed, extended with Klenow enzyme (Boehringer Mannheim), digested with *Nsi*I and *Apa*I and ligated into the NR1–SP expression plasmid.

NR2A subunit. Silent restriction sites *Spe*I and *Age*I encompassing the *C*-terminal side of the M2 domain were introduced by PCR. Mutants were generated by ligating appropriate oligonucleotides directly into the vector digested with *Spe*I–*Age*I. All restriction enzymes were obtained from New England Biolabs GmbH (Schwalbach, Germany).

Heterologous expression of NMDA receptor channels

NMDA receptor channels were heterologously expressed in *Xenopus* oocytes and HEK 293 cells. NR1 mutants were expressed together with wild-type NR2A or vice versa. Capped mRNA was transcribed for each expression construct using SP6 RNA polymerase (80 U μl^{-1}; Promega, Madison, WI, USA) and examined electrophoretically on a denaturating agarose gel. The concentration of the RNA was determined by ethidium bromide stain of the gel relative to an RNA standard ladder. Appropriate dilutions were prepared (0·01–1 $\mu g\ \mu l^{-1}$) in order to achieve optimal expression. *Xenopus* oocytes taken from frogs anaesthetized in an ice bath containing 0·3% MS-222 for 40 min were injected with 20–40 nl RNA solution using a Nanoject (Drummond Corp., Broomall, PA, USA) injector and were prepared and maintained as described previously (Raditsch *et al.* 1993). Outside-out macropatches were isolated 3–8 days after injection (Methfessel, Witzemann, Takahashi, Mishina, Numa & Sakmann, 1986).

HEK 293 cells (reference no. CRL 1573) were transiently transfected with vectors for NR1- and NR2A-subunits. In order to detect transfected cells, a vector for green fluorescent protein (Chalfie, Tu, Euskichen, Ward & Prasher, 1994) was co-transfected at a ratio of 1 : 6. Whole-cell recordings were made 2 days after transfection.

Solutions

Internal. For outside-out macropatches isolated from *Xenopus* oocytes, the pipette solution consisted of (mM): 100 KCl, 10 Hepes, and 10 BAPTA; pH adjusted to 7·2 with KOH. The total K^+ concentration was 123·5 mM. To record whole-cell currents in HEK 293 cells, the pipette solution consisted of (mM): 140 CsCl, 10 Hepes, and 10 EGTA; pH adjusted to 7·2 with CsOH. The total Cs^+ concentration was 163·5 mM. Hepes and EGTA were obtained from Carl Roth GmbH (Karlsruhe, Germany) and BAPTA from Sigma Chemical Co.

External. For oocyte macropatches, a KCl solution was used as a reference to measure permeability ratios (mM): 100 KCl, 10 Hepes, and 0·18 $CaCl_2$; pH adjusted to 7·2 with KOH. The total K^+ concentration was 103·5 mM. For HEK 293 cells, a CsCl solution was used as a reference (mM): 140 CsCl, and 10 Hepes; pH adjusted to 7·2 with CsOH. The total Cs^+ concentration was 143·5 mM. In test organic solutions, the 103·5 mM KCl or 143·5 mM CsCl was replaced by various test cations as the chloride salt (100 or 140 mM) and 10 mM histidine normally replaced Hepes as the buffer (pH adjusted to 7·2 with HCl); for the Tris and a tetraethylammonium (TEA) solution, Hepes was used as the buffer with the pH adjusted to 7·2 using HCl (Tris) or TEAOH (TEA). The following solution was used to measure Ca^{2+} permeability (mM): 1 $CaCl_2$, 100 *N*-methyl-D-glucamine (NMDG), and 10 Hepes; pH adjusted to 7·2 with HCl; at times 1 mM flufenamic acid, a blocker of the endogenous Ca^{2+}-activated chloride conductance, was added to this solution. All test cations and glutamate and glycine were obtained from Sigma Chemical Co. Stock solutions of glutamate (free acid) were adjusted to pH 7·2 using NMDG.

Current recordings and data analysis

Currents in oocyte outside-out macropatches or whole-cell currents in HEK 293 cells were recorded at room temperature (19–23 °C) with the patch clamp technique (Hamill, Marty, Neher, Sakmann & Sigworth, 1981). Pipettes were pulled from borosilicate glass and had resistances of 1–5 MΩ when filled with the pipette solution and measured in the K^+ or Cs^+ reference solutions. Current was measured using an EPC-9 with PULSE software (HEKA Electronics GmbH, Lambrecht, Germany), low-pass filtered at 1 kHz, and digitized at 2·5 kHz; for display, voltage ramps were refiltered at 100 Hz. External solutions were applied using a Piezo-driven double-barrel application system (Colquhoun, Jonas & Sakmann, 1992) with one barrel containing the external solution and the other barrel the same solution plus 100 μM glutamate and 10 μM glycine. Glutamate-activated current flowing through NMDA receptor channels was defined as the difference between currents recorded in the presence and absence of glutamate/glycine. For outside-out macropatches, voltage ramps (~80 mV s^{-1}) were used to determine the potential dependence of currents when recording in test organic solutions. Only patches with at least 2 GΩ seal resistance in the K^+ reference solution were used for voltage ramps; since the leak current is carried predominantly by K^+, in test organic solutions the corresponding seal resistance was greater than 30 GΩ. For currents in 1 mM Ca^{2+} as well as for all whole-cell recordings, voltage steps were used in 5 or 10 mV increments; the membrane potential was stepped to the test potential for 100 ms and then glutamate was rapidly applied for 25–50 ms (outside-out patches) or 200–300 ms (whole cell). To quantify zero-current (reversal) potentials, the reversal potential was estimated for glutamate-activated currents and then a third-order polynomial was fitted from ± 20 mV of the estimated reversal potential using Igor Pro (WaveMetrics, Inc., Lake Oswego, OR, USA).

Liquid junction potentials were measured using a pipette filled with 3 M KCl and were corrected during data analysis. The junction potential between the 103·5 mM K^+ reference solution and the KCl pipette solution was −2 mV (pipette negative), whereas that between the 143·5 mM Cs^+ reference solution and the CsCl pipette solution was −0·9 mV. Rapid application of test cation solutions generated junction potentials between the ground electrode and reference solution of −0·2 mV (ammonium, NH_4^+), −2·6 mV (methylammonium, MA), −3·7 mV (100 mM dimethylammonium, DMA), −3·9 mV (140 mM DMA), −6·1 mV (100 mM diethylammonium, DEA), −6·3 mV (140 mM DEA), −5·9 mV (dimethylethanolammonium, DMEtOHA), −4·7 mV (tetramethylammonium, TMA), −8 mV (Tris), −7·5 mV (TEA), and −8·7 mV (1 mM $CaCl_2$) (ground electrode 0 mV).

Reversal potentials were measured as follows. Glutamate-activated currents were initially measured in the 103·5 mM K^+ reference solution, and subsequently measured in a test solution. In most instances we then retested the K^+ reference solution. When compared with the first reference value, the second reference value never changed by more than 2 mV. When both pre- and

Table 1. ΔE_r and permeability ratios for Ca^{2+} measured in wild-type and mutant NR1–NR2A NMDA receptor channels

Subunit composition	$[Ca^{2+}]$ (mM)	ΔE_r (mV)	n	P_{Ca}/P_K	P_{Ca}*
NR1–NR2A	0·18	−102 ± 1·3	6	2·7	2·7
NR1–NR2A	1	−37·0 ± 0·5	8	7·2	2·7
NR1(N598G)–NR2A	1	−70·5 ± 1·0	5	1·7	0·6
NR1(N598S)–NR2A	1	~−107	4	0·4	0·2
NR1(N598D)–NR2A	1	−36·6 ± 0·2	4	7·3	2·7
NR1(N598Q)–NR2A	1	~−82	5	1·1	0·4
NR1(S599G)–NR2A	1	−38·7 ± 0·3	5	6·7	2·5
NR1(S599N)–NR2A	1	−39·3 ± 0·4	5	6·5	2·4
NR1(G600S)–NR2A	1	−36·8 ± 0·6	4	7·2	2·7
NR1–NR2A(N595G)	1	−40·0 ± 0·4	3	6·2	2·3
NR1–NR2A(N595S)	1	−40·6 ± 0·4	4	6·1	2·3
NR1–NR2A(N595D)	1	−40·0 ± 0·3	5	6·3	2·4
NR1–NR2A(N595Q)	1	−46·3 ± 0·5	4	4·7	1·8
NR1–NR2A(N596G)	1	−57·4 ± 0·7	4	2·9	1·1
NR1–NR2A(N596S)	1	−52·3 ± 0·7	6	3·6	1·4
NR1–NR2A(N596D)	1	−36·8 ± 0·2	4	7·2	2·7
NR1–NR2A(N596Q)	1	−44·8 ± 0·8	4	5·0	1·9
NR1–NR2A(S597G)	1	−47·3 ± 0·7	6	4·5	1·7
NR1–NR2A(S597N)	1	−38·7 ± 0·7	3	6·6	2·5
NR1(598Q)–NR2A(595Q)	1	~−64	2	2·2	0·8
NR1(598G)–NR2A(596G)	1	~−55	4	3·3	1·2

Reference solution (mM): 103·5 KCl, 10 Hepes, 0·18 $CaCl_2$; test solution (mM): 0·18 mM $CaCl_2$, 100 mM TMA, 10 mM histidine or 1 mM $CaCl_2$, 100 mM NMDG, 10 mM Hepes. * P_{Ca} is the value used in the Lewis equation to calculate permeability ratios for the particular subunit composition and is derived from the relationship:

$$P_{Ca} = 2{\cdot}7(P_{Ca,mutant}/P_{Ca,wild\ type}),$$

where $P_{Ca,mutant}$ and $P_{Ca,wild\ type}$ are the Ca^{2+} permeabilities measured in 1 mM Ca^{2+} (see Methods). Values of ΔE_r are means ± S.E.M.

postreference reversal potentials were measured, they were averaged when calculating changes in reversal potential induced by the test solution. A similar protocol was used to measure reversal potentials in whole-cell recordings of HEK 293 cells. Results are reported as means ± S.E.M. A single-factor ANOVA was used to test for statistical significance of differences in permeability ratios between different subunit combinations with the Tukey test used for multiple comparisons. A significance was assumed if $P < 0{\cdot}05$.

Ionic selectivity. Permeability ratios were determined using the Lewis equation (Lewis, 1979) which is derived from the Goldman–Hodgkin–Katz (GHK) current equation and which takes into account the presence of more than one permeant ion of differing valence. For NMDA receptor channels, which are permeable to monovalent alkali cations as well as Ca^{2+}, this equation has the generalized form in physiological solutions of:

$$E_r = \frac{RT}{F}\ln\frac{[K^+]_o + \frac{P_{Na}}{P_K}[Na^+]_o + 4\frac{P'_{Ca}}{P_K}[Ca^{2+}]_o}{[K^+]_i + \frac{P_{Na}}{P_K}[Na^+]_i + 4\frac{P'_{Ca}}{P_K}[Ca^{2+}]_i \exp(E_r F/RT)}, \quad (1)$$

where E_r is the zero-current or reversal potential and P'_{Ca} is $P_{Ca}/(1 + \exp(E_r F/RT))$. R, T and F have their normal thermodynamic meanings and the quantity RT/F was 25·4 mV (21 °C).

For outside-out macropatches, all external solutions contained 0·18 mM $CaCl_2$ to prolong the lifetime of the patch. With K^+ and Ca^{2+} as the only external permeant ions and K^+ as the only internal permeant ion, the Lewis equation has the form:

$$E_r = \frac{RT}{F}\ln\frac{[K^+]_o + 4\frac{P'_{Ca}}{P_K}[Ca^{2+}]_o}{[K^+]_i}. \quad (2)$$

Ionic selectivity of NMDA receptor channels was determined by measuring the change of reversal potential for glutamate-activated currents on replacing the 103·5 mM K^+ reference solution with a similar solution except that the K^+ was replaced by a test cation, X^+. Permeability ratios, P_X/P_K, were calculated according to the relationship:

$$E_{r,X} - E_{r,K} = \frac{RT}{F}\ln\frac{\frac{P_X}{P_K}[X^+]_o + 4\frac{P''_{Ca}}{P_K}[Ca^{2+}]_o}{[K^+]_o + 4\frac{P'_{Ca}}{P_K}[Ca^{2+}]_o}, \quad (3)$$

where P'_{Ca} is $P_{Ca}/(1 + \exp(E_{r,K}F/RT))$ and P''_{Ca} is $P_{Ca}/(1 + \exp(E_{r,X}F/RT))$. These are the Ca^{2+} correction terms reflecting the presence of external Ca^{2+} in the reference and test solutions, respectively (see below). Hence, permeability ratio calculations using changes of reversal potential require an absolute

reversal potential for the reference and test solutions reflecting the fact that the primed P_{Ca} term is voltage dependent. For all calculations we assumed that the unprimed P_{Ca}/P_K was the same in reference and test solutions.

For HEK 293 cells, whole-cell recordings were made in the absence of external Ca^{2+}. Hence, with Cs^+ as the reference solution and again using changes in reversal potentials, eqn (3) simplifies to the bi-ionic equation (Hille, 1992):

$$E_{r,X} - E_{r,Cs} = \frac{RT}{F} \ln \frac{\frac{P_X}{P_{Cs}}[X^+]_o}{[Cs^+]_o}. \quad (4)$$

Correction factor for Ca^{2+} permeability. The focus of the present work was to define the molecular determinants of the narrow constriction of the NMDA receptor channel. Nevertheless, wild-type NMDA receptor channels are permeable to Ca^{2+} and many of the mutations changed this Ca^{2+} permeability. Therefore, to calculate permeability ratios, we needed an estimate of the Ca^{2+} permeability for wild-type and all mutant channels. For wild-type NMDA receptor channels, we found a small but consistent inward current when TMA was present externally as the test cation (Fig. 1*D*). Since TMA is impermeant in recombinant NR1–NR2A NMDA receptor channels (Villarroel *et al.* 1995), we assumed that this inwardly directed current reflects a small Ca^{2+} flux and used the reversal potential in this solution as a measure of Ca^{2+} permeability. To calculate P_{Ca}/P_K we again used changes in reversal potential and the Lewis equation (eqn (3)), which, assuming TMA is impermeant, simplifies to:

$$E_{r,Ca} - E_{r,K} = \frac{RT}{F} \ln \frac{4\frac{P''_{Ca}}{P_K}[Ca^{2+}]_{test}}{[K^+]_o + 4\frac{P'_{Ca}}{P_K}[Ca^{2+}]_o}, \quad (5)$$

where $[Ca^{2+}]_{test}$ is 0·18 mM and P'_{Ca} and P''_{Ca} have the same meaning as in eqn (3). Using this approach, we obtained a P_{Ca}/P_K value in 0·18 mM $CaCl_2$ of 2·7 (Table 1).

To measure P_{Ca}/P_K for the mutant channels, we did not use the 0·18 mM $CaCl_2$, 100 mM TMA solution. First, inward currents in 0·18 mM Ca^{2+} are at the limit of resolution of our recordings, and in mutations where the Ca^{2+} permeability is decreased, a reliable reversal potential would be difficult to measure. In addition, mutations which make the pore size larger could also allow TMA to permeate the channel. To circumvent these problems, we measured P_{Ca}/P_K for wild-type and each mutant channel using an external solution containing 1 mM $CaCl_2$ and the much larger organic cation NMDG. We did not use a higher concentration of external Ca^{2+} since even in 1 mM Ca^{2+} the endogenous Ca^{2+}-activated chloride conductance occasionally contaminated recordings of NMDA receptor-mediated currents despite the presence of 10 mM BAPTA in the recording pipette and brief applications of glutamate (25–50 ms).

Using the 1 mM $CaCl_2$, NMDG solution, and eqn (5) where $[Ca^{2+}]_{test}$ is 1 mM, we obtained a P_{Ca}/P_K value for wild-type NMDA receptor channels of 7·2 (Table 1). The two solutions used to measure P_{Ca}/P_K in wild-type NMDA receptor channels gave different P_{Ca} values: in 0·18 mM Ca^{2+}, 100 mM TMA the value was 2·7 whereas in 1 mM Ca^{2+}, 100 mM NMDG it was 7·2. Measurement of P_{Ca}/P_K in HEK 293 cells using 0·18 mM Ca^{2+} plus 140 mM NMDG and 1 mM Ca^{2+} plus 140 mM NMDG has shown a similar disparity (2·4 *vs.* 7·1, respectively; L. P. Wollmuth & D.-S. Koh, unpublished observations). Hence, we used the P_{Ca} value measured in 0·18 mM Ca^{2+} to calculate permeability ratios since the Ca^{2+} concentration is the same as that used in all experiments. Therefore, to calculate P_{Ca} for the mutant channels in solutions containing 0·18 mM $CaCl_2$ we used the following relationship:

$$P_{Ca} = 2{\cdot}7\,(P_{Ca,mutant}/P_{Ca,wild\ type}),$$

where $P_{Ca,mutant}$ and $P_{Ca,wild\ type}$ are the Ca^{2+} permeabilities measured in 1 mM Ca^{2+}. This approach assumes that the ratio between P_{Ca} in mutant and wild-type channels in 0·18 and 1 mM Ca^{2+} is similar; this assumption seems justified since the ratio of the Ca^{2+} permeability for mutant relative to wild-type channels measured in 110 mM Ca^{2+} (L. P. Wollmuth, unpublished data) is similar to the corresponding ratio measured in 1 mM Ca^{2+}.

To assess our approach of calculating permeability ratios in oocyte macropatches, we measured organic cation permeability in wild-type and several mutant NMDA receptor channels in HEK 293 cells where external Ca^{2+} is not required for whole-cell recordings. Here CsCl was used as a reference solution to minimize current flowing through K^+ channels. For HEK 293 cells expressing NR1–NR2A channels, the mean permeability ratios were: P_{DMA}/P_{Cs}, 0·18; and P_{DEA}/P_{Cs}, 0·07; which when converted to values relative to K^+ were 0·20 and 0·08, values very similar to those derived from oocyte macropatches (Table 2). Similarly, for the mutant channels NR1–NR2A(595D) and NR1–NR2A(N596S), their DMA permeability relative to that in wild-type channels showed a quantitative agreement with those determined in oocytes (asterisks, Fig. 6, lower panel).

RESULTS

To determine which amino acids contribute to the narrow constriction, we compared the permeability of differently sized organic cations in wild-type and mutant NMDA receptor channels. We first quantified the permeability of organic cations in wild-type NMDA receptor channels.

Selectivity of the wild-type NR1–NR2A NMDA receptor channel

Figure 1 shows glutamate-activated currents produced by voltage ramps in outside-out macropatches isolated from oocytes expressing recombinant NR1–NR2A NMDA receptor channels. In Fig. 1*A*, the currents in the K^+ reference solution are shown from −62 to +58 mV and cross the voltage axis at −5·1 mV, defining the reversal potential. When external K^+ was replaced by the organic cation DMA, the current reversal was shifted towards more negative potentials by nearly 40 mV, indicating that DMA is less permeant than K^+ and yielding a mean permeability ratio P_{DMA}/P_K of 0·20 ($n = 10$; Table 2). When K^+ was replaced by the larger organic cations DEA (Fig. 1*B*) or DMEtOHA (Fig. 1*C*), the reversal potentials for the currents were shifted negative by approximately 63 and 86 mV, respectively, giving permeability ratios P_{DEA}/P_K of 0·07 and $P_{DMEtOHA}/P_K$ of 0·02 ($n = 9$ for each). Table 2 summarizes the changes in reversal potential and permeability ratios for DMA, DEA and DMEtOHA as well as NH_4^+ and MA in wild-type channels. Also shown in Table 2 are the dimensions of the organic cations. Consistent

with the size of the organic cation affecting its permeability, the permeability of the organic cation decreases as additional or larger side groups are added to the core ammonium.

Mutation of the N-site asparagine to glutamine in either the NR1- or NR2A-subunit changes the permeability of organic cations but in an asymmetrical manner

In both the NR1- and NR2A-subunits, mutation of an asparagine at the N-site to glutamine produces strong effects on divalent reversal potentials, suggesting that amino acids at these sites contribute to the permeation pathway of the NMDA receptor channel (Burnashev *et al.* 1992). This also suggests that the asparagines at the N-sites may contribute to the narrow constriction. Figure 2 shows glutamate-activated currents for mutant NMDA receptor channels with the N-site asparagine (N) changed to the larger glutamine (Q) in either the NR1-subunit (Fig. 2*B* and *C*) or the NR2A-subunit (Fig. 2*D* and *E*). For NR1(N598Q)–NR2A mutant channels, when external K^+ was replaced by DMA (Fig. 2*B*), the current reversal was shifted negative by 36 mV rather than the 40 mV shift seen for wild-type channels, indicating that DMA can more readily permeate the mutant channel. Correspondingly, the calculated P_{DMA}/P_K of 0·25 ($n = 6$; Table 3) was larger than the value of 0·20 found for wild-type channels. When

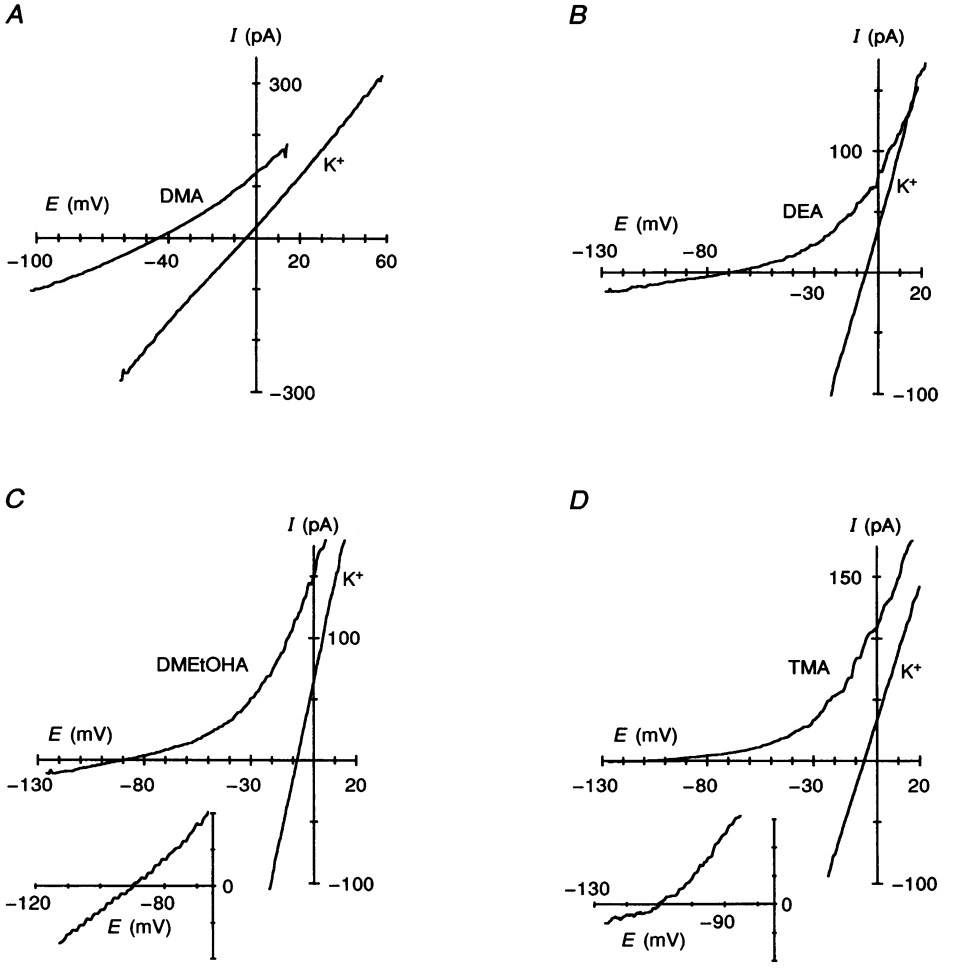

Figure 1. Reversal of glutamate-activated currents in wild-type NR1–NR2A NMDA receptor channels

A–D, glutamate-activated currents in outside-out patches from *Xenopus* oocytes expressing the wild-type NR1- and NR2A-subunits. Currents were generated by voltage ramps (~80 mV s^{-1}) and were recorded in the presence of the K^+ reference solution or a solution in which the K^+ was replaced by dimethylammonium (DMA; *A*), diethylammonium (DEA; *B*), dimethylethanolammonium (DMEtOHA; *C*) or tetramethylammonium (TMA; *D*). The K^+ records are an average of the currents recorded before and after exposure to the organic cation. In *A*, the currents in the presence of K^+ are displayed from −62 to +58 mV; although all K^+ reference recordings were made over this voltage range, for clarity in *B–D* and all subsequent figures, the currents in the presence of K^+ are nominally shown only from −20 to +20 mV. The insets in *C* and *D* expand the current traces in the presence of the organic ion to show current reversal; the current scale extends from −10 to +10 pA (inset to *C*) or −2 to +3 pA (inset to *D*).

Table 2. ΔE_r and permeability ratios for organic cations measured in wild-type NR1–NR2A NMDA receptor channels

X	ΔE_r (mV)	n	P_X/P_K	P_X/P_{Cs}	Dimensions (nm)	(nm^2)
A. Oocyte outside-out macropatches using voltage ramps						
K^+	0	—	1·0	—	—	
NH_4^+	5·3 ± 0·4	5	1·28	—	0·33 × 0·32 × 0·34	(0·106)
MA	−18·7 ± 0·4	8	0·48	—	0·35 × 0·375 × 0·41	(0·131)
DMA	−39·6 ± 0·2	10	0·20	—	0·38 × 0·42 × 0·61	(0·16)
DEA	−61·8 ± 1·4	9	0·07	—	0·39 × 0·44 × 0·85	(0·172)
DMEtOHA	−85·2 ± 0·9	9	0·02	—	0·42 × 0·55 × 0·71	(0·231)
TMA	−102 ± 1·3	6	—	—	0·55 × 0·55 × 0·55	(0·303)
Tris	—	—	—	—	0·55 × 0·56 × 0·64	(0·308)
TEA	—	—	—	—	0·58 × 0·70 × 0·70	(0·406)
B. Whole-cell recordings of HEK 293 cells using voltage steps						
Cs^+	0	—	—	1·0	—	
DMA	−44·0 ± 0·8	8	0·20	0·18	—	
DEA	−66·3 ± 0·3	5	0·08	0·075	—	

Values of ΔE_r are means ± S.E.M. A, reference solution (mM): 103·5 KCl, 10 Hepes, 0·18 $CaCl_2$; test solution (mM): 100 XCl, 10 histidine, 0·18 $CaCl_2$. Permeability ratios were calculated using eqn (3) assuming $P_{Ca}/P_K = 2·7$ (see Methods). Dimensions of organic cations were determined by the smallest size box that would contain Corey–Pauling space-filling models of the molecule; the values in parentheses are the cross-sectional area of the two smallest dimensions. B, reference solution (mM): 143·5 CsCl, 10 Hepes; test solution (mM): 140 XCl, 10 histidine. Permeability ratios were calculated using eqn (4) and were changed relative to K^+ using $P_{Cs}/P_K = 1·12$ (Tsuzuki, Mochizuki, Iino, Mori, Mishina & Ozawa, 1994).

the larger organic cation DEA replaced K^+ (Fig. 2*C*), the shift in the reversal potential was again less than that seen for wild-type channels but the difference of nearly 16 mV between the shift for wild-type and mutant channels was much greater than that seen for DMA and produced more than a two-fold increase in P_{DEA}/P_K, from 0·07 to 0·17 ($n = 4$). In contrast, a different pattern was seen with the same asparagine to glutamine mutation in the N-site of the NR2A-subunit. As observed for the NR1(N598Q)–NR2A mutant channels, the shift in the reversal potential on replacing K^+ by DMA was less than that seen for wild-type channels (Fig. 2*D*). However, when the larger DEA replaced K^+, the shift in the reversal potential was nearly identical to that found in wild-type channels (Fig. 2*E*).

To examine further the relationship between the size of the organic cation and its permeability in the two mutant

Table 3. ΔE_r and permeability ratios for organic cations measured in NR1–NR2A NMDA receptor channels with the N-site asparagine (N) mutated to a glutamine (Q)

Subunit composition	X	ΔE_r (mV)	n	P_X/P_K
	K^+	0	—	1·0
NR1(N598Q)–NR2A	MA	−18·4 ± 0·2	5	0·50
	DMA	−36·1 ± 0·5	6	0·25
	DEA	−45·5 ± 1·5	4	0·17
	DMEtOHA	−63·9 ± 0·9	4	0·08
NR1–NR2A(N595Q)	MA	−13·7 ± 0·3	5	0·60
	DMA	−36·5 ± 0·6	6	0·24
	DEA	−60·3 ± 0·9	5	0·09
	DMEtOHA	−92·7 ± 0·5	4	0·01
NR1(N598Q)–NR2A(N595Q)	MA	−11·2 ± 0·1	6	0·66
	DMA	−28·8 ± 0·2	5	0·33
	DEA	−38·7 ± 0·1	5	0·22
	DMEtOHA	−56·9 ± 0·5	5	0·11

Reference solution (mM): 103·5 KCl, 10 Hepes, 0·18 $CaCl_2$; test solution (mM): 100 XCl, 10 histidine, 0·18 $CaCl_2$. Permeability ratios were calculated using eqn (3). Values of ΔE_r are means ± S.E.M.

channels, we also measured the permeability of MA, which is smaller than DMA, and of DMEtOHA, which is larger than DEA (Table 3; Fig. 3*A* and *B*). For the NR1(N598Q)–NR2A channels (Fig. 3*A*, ○), there was a greater divergence in P_X/P_K values as the size of the test organic cation became larger: for MA there was essentially no difference between mutant and wild-type channels whereas for DEA and DMEtOHA there was a 2·3- and 4·5-fold increase in permeability, respectively. In contrast, the NR1–NR2A (N595Q) mutant channels (Fig. 3*B*, ◇) showed the opposite result: a significant increase in the MA and DMA permeabilities ($P < 0·05$) but no significant difference for those for DEA or DMEtOHA.

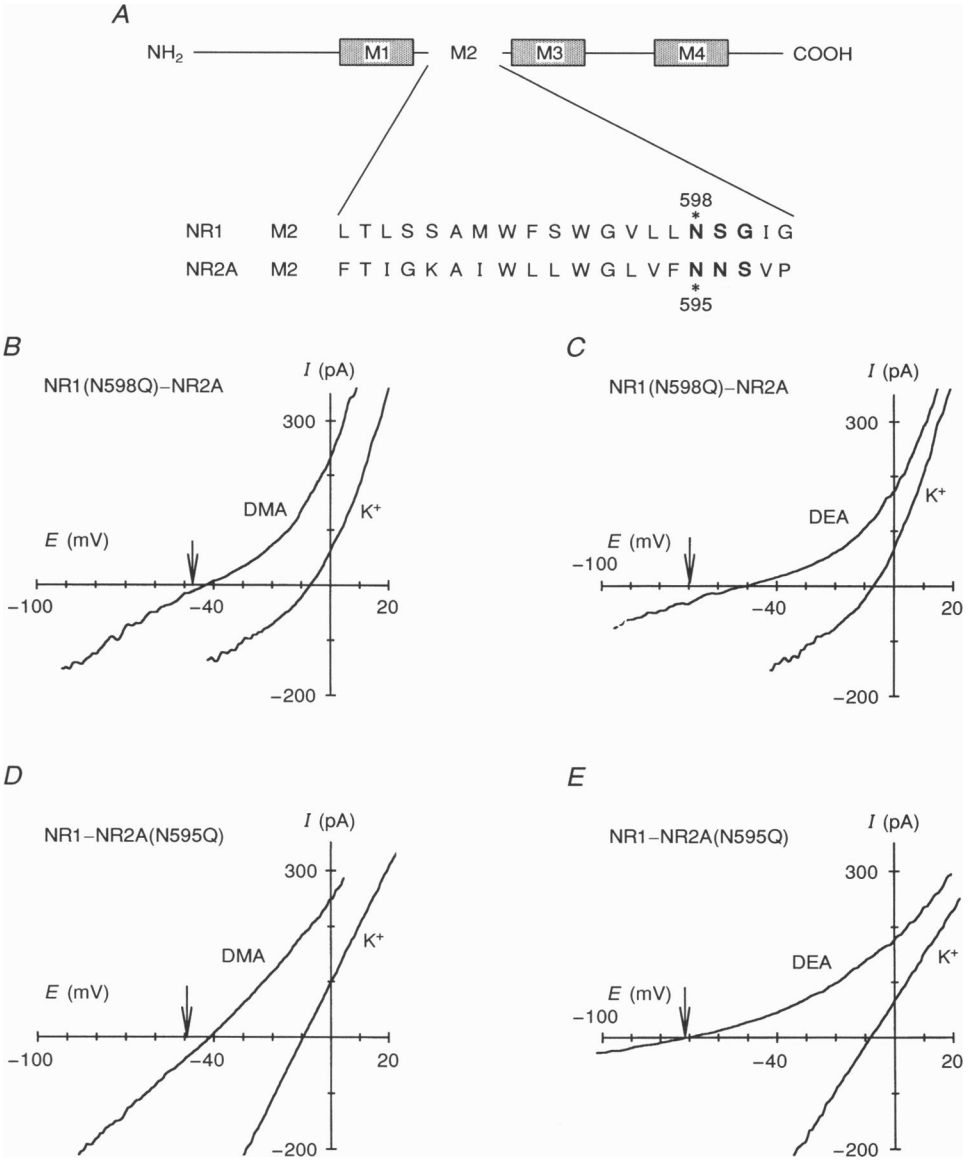

Figure 2. Mutation of the N-site asparagine (N) to glutamine (Q) in either the NR1- or NR2A-subunit changes the reversal potential of organic cations relative to that in wild-type channels

A, amino acid sequence of the putative pore-forming domain (M2) of the wild-type NR1- and NR2A-subunits. The N-site, homologous to the Q/R-site in AMPA receptors, is indicated by an asterisk. *B–E*, glutamate-activated currents were recorded and displayed as in Fig. 1 except that macropatches were isolated from oocytes expressing either a mutated form of the NR1-subunit, in which the asparagine (N) at position 598 was mutated to a glutamine (Q), and the wild-type NR2A-subunit (NR1(N598Q)-NR2A; *B* and *C*); or the wild-type NR1-subunit and the same N-site mutation in the NR2A-subunit (NR1–NR2A(N595Q); *D* and *E*). The arrows in *B–E*, as well as those in Figs 4, 5 and 7, indicate the expected reversal potential for the organic cation given the observed reversal potential in the K^+ reference solution and the average change in reversal potential for that organic cation in wild-type NR1–NR2A NMDA receptor channels (Table 2).

How can we interpret these two patterns of increasing organic cation permeability relative to wild-type channels? In the case of NR1(N598Q)–NR2A channels, the greater relative difference in permeability with increasing size of the organic cation is what we will interpret as an increase in the size of the narrow constriction. Organic cations much smaller than the narrow constriction, such as MA, would be relatively insensitive to changes in pore size whereas larger organic cations, such as DEA and DMEtOHA, which only poorly traverse the narrow region, would be more sensitive. Hence, the increased organic cation permeability seen for the NR1–NR2A(N595Q) channels, where a significant change occurs only for the smaller organic cations MA and DMA, would not reflect a change in the pore size but rather a change in some other permeation property, most probably binding affinity.

The NR1(N598Q)–NR2A(N595Q) mutant channel increases the permeability of organic cations more than each individual mutant channel

It was surprising to find that the NR1(N598Q)–NR2A mutant channels had an increased pore size since glutamine is a larger amino acid than the native asparagine and hence should decrease the pore size. One possibility is that the native asparagines are packed tightly in the narrow constriction and that the bulkier side chain of glutamine may disrupt the normal structure. If this is true, and since the N-sites for the two subunits are probably located close

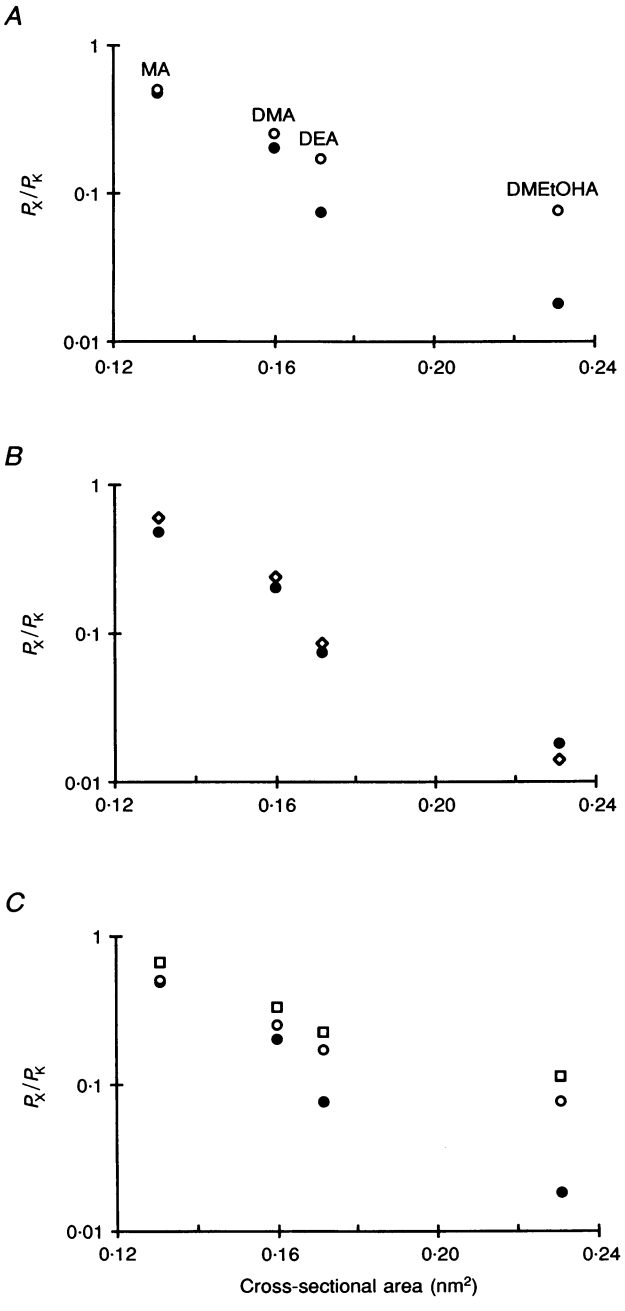

Figure 3. Glutamine at the N-site in the NR1- or NR2A-subunit produces different patterns of changes in organic cation permeability

Permeabilities of MA, DMA, DEA and DMEtOHA in NR1(N598Q)–NR2A (*A*, ○), NR1–NR2A(N595Q) (*B*, ◇) and NR1(N598Q)–NR2A(N595Q) (*C*, □) mutant channels are plotted as a function of the cross-sectional area of the two smallest dimensions of the organic cation (see Table 2). In each plot ● indicates the corresponding values for wild-type channels (Table 2). In *C*, permeabilities in NR1(N598Q)– NR2A mutant channels (○) are shown for comparison.

to each other (see Discussion), the presence of a bulkier side chain at the N-site for both subunits should have a stronger effect on increasing pore size. Indeed, as shown in Fig. 3*C* (□), the permeability of all four organic cations for the double-mutant channel, NR1(N598Q)–NR2A(N595Q), was greater than that for either of the individual mutant channels (Table 3). For MA and DMA this difference is ambiguous since it may reflect an increase in the pore size as well as a change in binding properties. However, in the NR2A(N595Q) mutant channels the permeabilities of the larger organic cations DEA and DMEtOHA were not significantly affected, yet the double mutation significantly increased P_{DEA}/P_K to 0·22 and $P_{DMEtOHA}/P_K$ to 0·11 compared with values of 0·17 and 0·08, respectively, for the NR1(N598Q) mutant channels. Hence, the observation that the pore size of the double-mutant channel increased more than that of the channel with the NR1(N598Q) individual mutation further supports the idea that the presence of the bulkier side chain at the NR1 N-site disrupts the normal narrow constriction.

A glycine in the N-site of the NR1- but not the NR2A-subunit strongly increases organic cation permeability

The results for the asparagine to glutamine mutations suggested that the N-sites of the two subunits may be positioned differently in the channel lumen. Additional evidence for a structural asymmetry was obtained when the N-sites in either subunit contained the small and uncharged glycine (G) residue (Fig. 4). For NR1(N598G)–

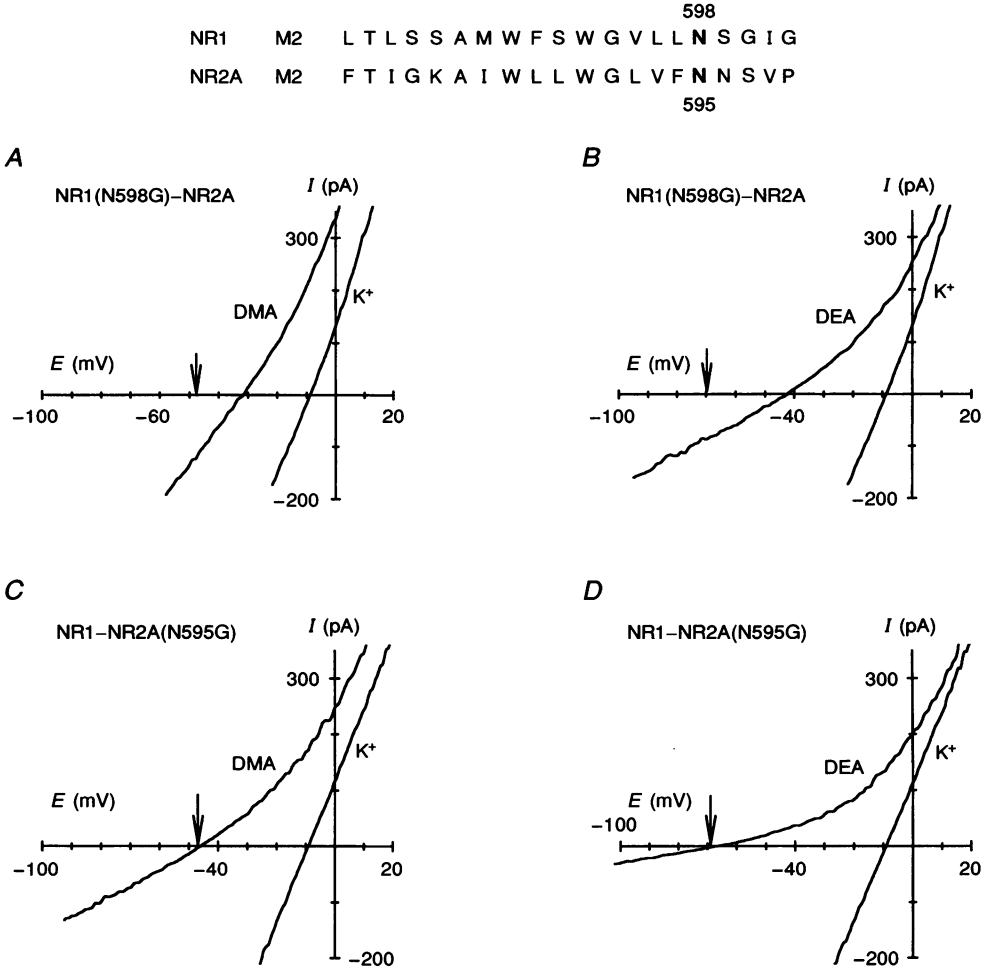

Figure 4. Mutation of the N-site asparagine (N) to the smaller glycine (G) in the NR1- but not in the NR2A-subunit shifts the reversal potential of organic cations in a strongly positive direction

Glutamate-activated currents were recorded and displayed as in Fig. 1 except that macropatches were isolated from oocytes expressing NR1(N598G)–NR2A (*A* and *B*) or NR1–NR2A(N595G) (*C* and *D*) mutant channels. The amino acid sequences of the wild-type NR1- AND NR2A-subunit M2 domains are shown at the top (see Fig. 2).

NR2A mutant channels, the shift in reversal potential on replacing external K^+ with DMA (Fig. 4*A*) or with DEA (Fig. 4*B*) was nearly 15 and 25 mV less, respectively, than that seen for wild-type channels, yielding permeability ratios P_{DMA}/P_K of 0·4 ($n = 6$) and P_{DEA}/P_K of 0·24 ($n = 6$), approximately 2 and 3·2 times larger than those found for wild-type channels (Table 4). In contrast, the same asparagine to glycine mutation in the NR2A N-site produced only small differences in the reversal potentials of DMA (Fig. 4*C*) and DEA (Fig. 4*D*) and a small but significant ($P < 0·05$) increase in P_{DMA}/P_K to 0·23 ($n = 6$) and P_{DEA}/P_K to 0·10 ($n = 6$; Table 5).

For the NR2A-subunit, mutation of the N + 1 site asparagine produces large and volume-specific effects on organic cation permeability

In contrast to the NR1 N-site, mutation of the NR2A N-site to smaller or larger sized amino acids had only small effects on organic cation permeability. However, much stronger effects were found when an asparagine occupying the N + 1 site in the NR2A-subunit was mutated. Figure 5 shows current records for mutant channels containing wild-type NR1-subunits and mutated forms of the NR2A-subunit in which the N + 1 site asparagine was changed to the smaller glycine (Fig. 5*A* and *B*) or the larger glutamine (Fig. 5*C* and *D*). For NR1–NR2A(N596G) mutant

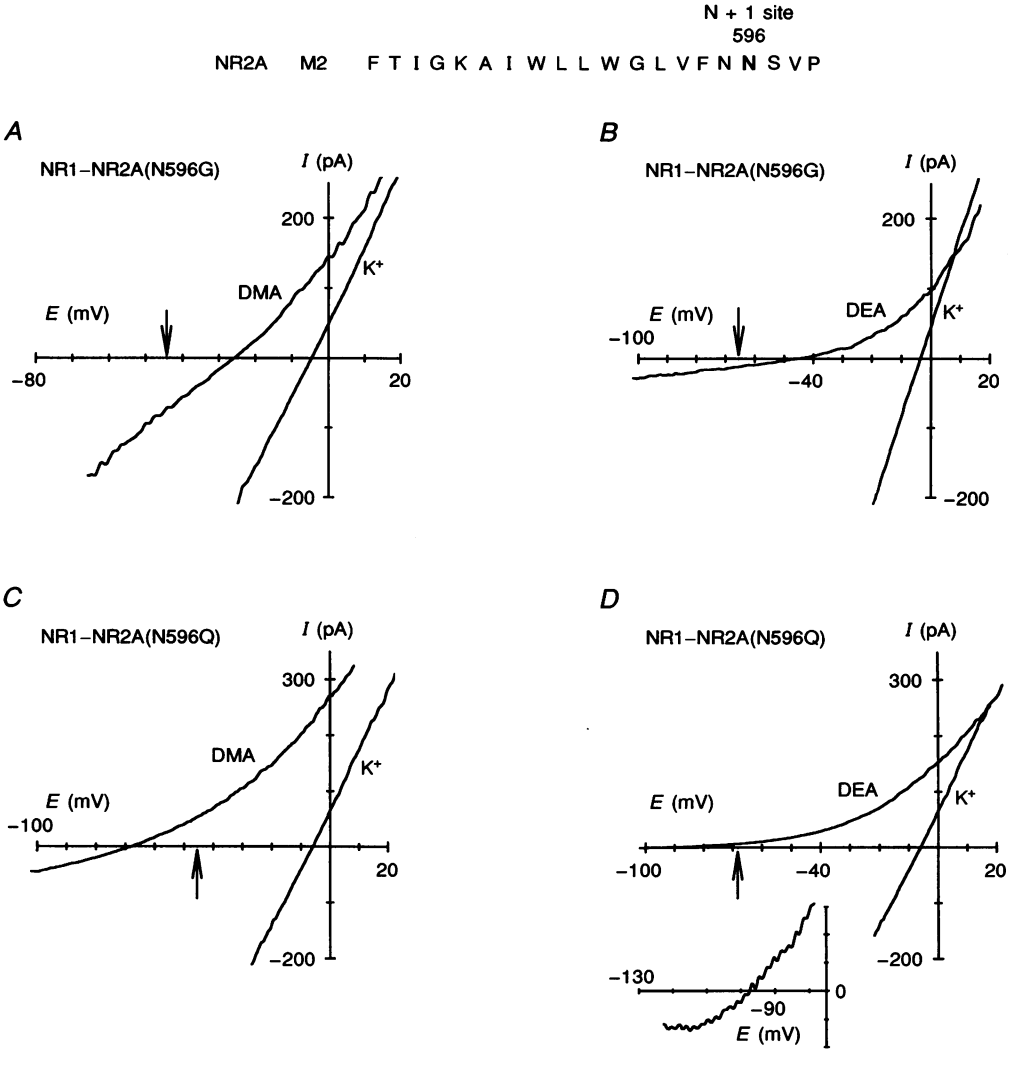

Figure 5. Mutation of the N + 1 site asparagine (N) in the NR2A-subunit produces large, volume-specific changes in the reversal potential of organic cations

Glutamate-activated currents were recorded and displayed as in Fig. 1 except that macropatches were isolated from oocytes expressing NR1–NR2A(N596G) (*A* and *B*) or NR1–NR2A(N596Q) (*C* and *D*) mutant channels. The amino acid sequence of the wild-type NR2A-subunit M2 domain is shown at the top (see Fig. 2). The inset in *D* expands the current trace in the presence of DEA to show current reversal; the current scale extends from −4 to +6 pA.

Table 4. ΔE_r and permeability ratios for organic cations measured in NMDA receptor channels composed of mutated NR1- and wild-type NR2A-subunits

Subunit composition	X	ΔE_r (mV)	n	P_X/P_K
	K^+	0	—	1·0
NR1(N598G)–NR2A	DMA	−24·2 ± 0·5	6	0·4
	DEA	−36·9 ± 1·0	6	0·24
NR1(N598S)–NR2A	DMA	−43·0 ± 0·5	5	0·19
	DEA	−63·0 ± 1·0	5	0·085
NR1(N598D)–NR2A	DMA	−44·7 ± 0·6	7	0·16
	DEA	−80·7 ± 1·0	4	0·025
NR1(N598R)–NR2A	DMA	−15·0 ± 0·3	5	0·57
NR1(S599G)–NR2A	DMA	−40·6 ± 0·8	5	0·2
	DEA	−64·4 ± 0·7	3	0·07
NR1(S599N)–NR2A	DMA	−34·9 ± 0·3	5	0·25
	DEA	−59·1 ± 1·2	5	0·09
NR1(G600S)–NR2A	DMA	−38·3 ± 0·3	5	0·215
	DEA	−61·2 ± 0·5	3	0·08

Reference solution (mM): 103·5 KCl, 10 Hepes, 0·18 $CaCl_2$; test solution (mM): 100 XCl, 10 histidine, 0·18 $CaCl_2$. Permeability ratios were calculated using eqn (3). Values of ΔE_r are means ± S.E.M.

Table 5. ΔE_r and permeability ratios for organic cations measured in NMDA receptor channels composed of wild-type NR1- and mutated NR2A-subunits

Subunit composition	X	ΔE_r (mV)	n	P_X/P_K	P_X/P_{Cs}
A. Oocyte outside-out macropatches using voltage ramps					
	K^+	0	—	1·0	—
NR1–NR2A(N595G)	DMA	−37·0 ± 0·4	6	0·23	—
	DEA	−56·7 ± 0·7	5	0·10	—
NR1–NR2A(N595S)	DMA	−34·5 ± 0·4	6	0·25	—
	DEA	−58·5 ± 0·7	5	0·09	—
NR1–NR2A(N595D)	DMA	−49·9 ± 1·3	4	0·13	—
	DEA	−69·7 ± 1·8	4	0·05	—
NR1–NR2A(N595R)	DMA	−64·9 ± 1·0	4	0·08	—
NR1–NR2A(N596G)	DMA	−23·0 ± 0·4	6	0·41	—
	DEA	−40·8 ± 0·7	5	0·20	—
NR1–NR2A(N596S)	DMA	−26·3 ± 0·5	6	0·36	—
	DEA	−40·6 ± 0·9	6	0·20	—
NR1–NR2A(N596D)	DMA	−38·5 ± 0·2	5	0·21	—
	DEA	−63·5 ± 0·5	5	0·07	—
NR1–NR2A(N596Q)	DMA	−63·6 ± 1·6	5	0·07	—
	DEA	−95·2 ± 1·8	5	0·01	—
NR1–NR2A(S597G)	DMA	−32·3 ± 0·5	5	0·28	—
	DEA	−47·3 ± 1·3	5	0·15	—
NR1–NR2A(S597N)	DMA	−32·0 ± 0·3	4	0·28	—
	DEA	−54·1 ± 1·0	5	0·11	—
B. Whole-cell recordings of HEK 293 cells using voltage steps					
	Cs^+	0	—	—	1·0
NR1–NR2A(N595D)	DMA	−52·7 ± 0·3	4	—	0·13
NR1–NR2A(N596S)	DMA	−28·7 ± 0·6	5	—	0·33

Values of ΔE_r are means ± S.E.M. A, reference solution (mM): 103·5 KCl, 10 Hepes, 0·18 $CaCl_2$; test solution (mM): 100 XCl, 10 histidine, 0·18 $CaCl_2$. Permeability ratios were calculated using eqn (3). B, reference solution (mM): 143·5 CsCl, 10 Hepes; test solution (mM): 140 XCl, 10 histidine. Permeability ratios were calculated using eqn (4).

channels, the shift in the reversal potential on replacing external K^+ with DMA (Fig. 5*A*) or with DEA (Fig. 5*B*) was nearly 17 and 21 mV less, respectively, than that seen for wild-type channels and gave a mean P_{DMA}/P_K of 0·41 ($n = 6$) and P_{DEA}/P_K of 0·20 ($n = 5$), values comparable to those found for the NR1(N598G)–NR2A mutant channels. On the other hand, when this asparagine was mutated to glutamine, the shift in the reversal potential on replacing K^+ with DMA (Fig. 5*C*) or with DEA (Fig. 5*D*) was more negative than that seen for the wild-type channels yielding values of P_{DMA}/P_K of 0·07 ($n = 5$) and P_{DEA}/P_K of 0·01 ($n = 5$), indicating that they permeate less well in this mutant channel.

The asparagines at the NR1 N-site and the NR2A N + 1 site contribute to the narrow constriction of NMDA receptor channels

Mutation of the N-site asparagine to glycine or glutamine in the NR1-subunit produced strong increases in the permeability of organic cations suggesting that this site contributes to the narrow constriction. To test this further, we measured the permeability of DMA and DEA in channels containing other mutations in the NR1-subunit. Figure 6 (upper panel) and Table 4 summarize these results. In Fig. 6, to compare the effect of mutations on organic cation permeability, we have displayed the results as $P_{X,mutant}/P_{X,wild\ type}$; in this form, an increase in the permeability relative to wild type gives a value greater than unity whereas a decrease gives a value less than unity. Again, mutation of the N-site asparagine to the smaller glycine or larger glutamine increased the permeability of DMA and DEA relative to wild-type channels with a much stronger relative effect on that of DEA. Replacing the asparagine with the smaller and polar serine was essentially without effect whereas when it was replaced with the negatively charged aspartate the permeability of both DMA and DEA decreased but again there was a stronger effect for DEA than for DMA. When the N-site

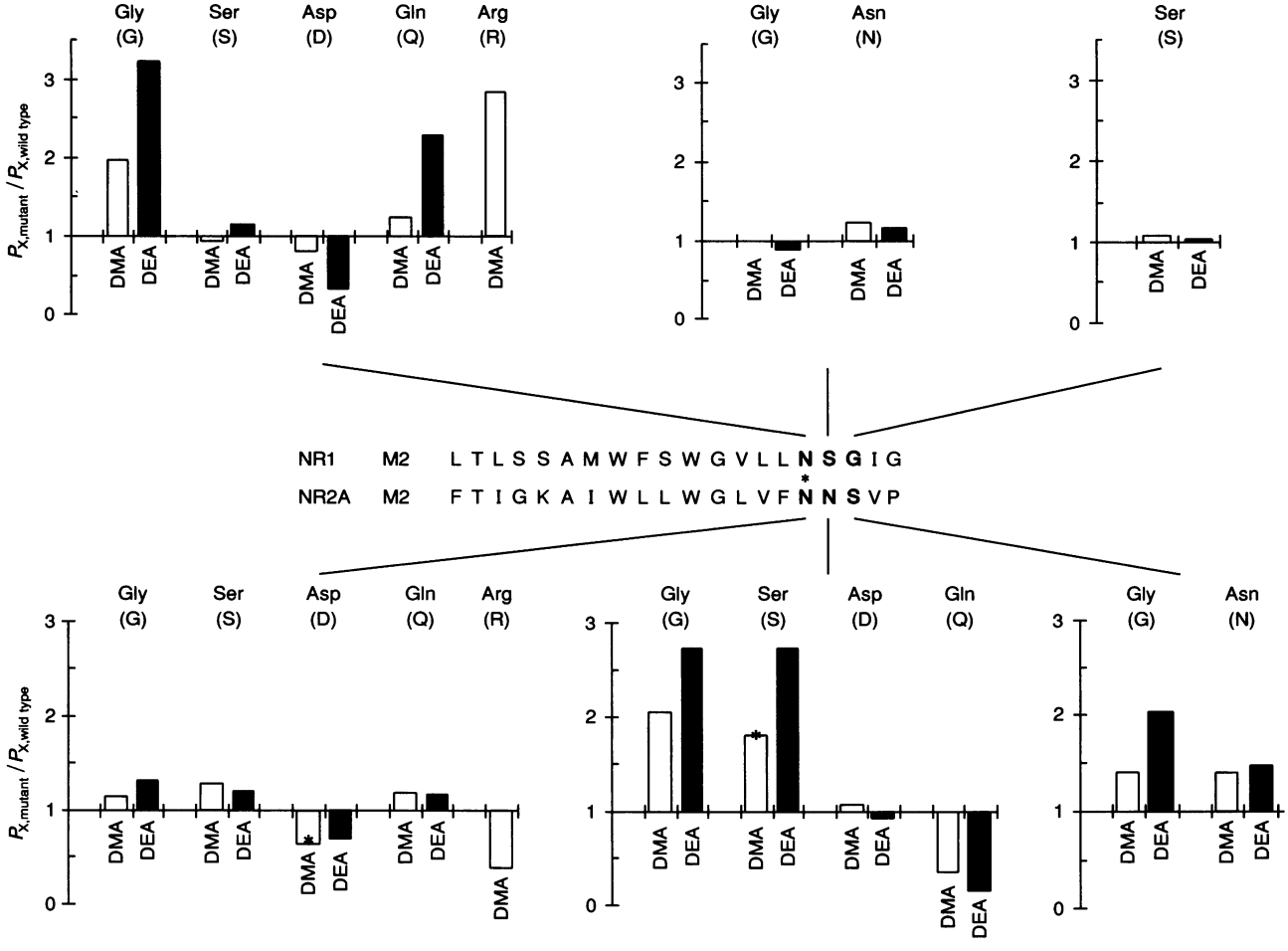

Figure 6. The asparagines at the NR1 N-site and the NR2A N + 1 site contribute to the narrow constriction of NMDA receptor channels

Summary of the effects of mutations in the NR1-subunit (upper panel) or the NR2A-subunit (lower panel) on the permeability of DMA and DEA relative to that in wild-type channels. For comparison, mutations are shown from left to right in increasing volume of the side chain. The position of the asterisks shows the same ratio measured in HEK 293 cells.

Table 6. ΔE_r and permeability ratios for organic cations measured in NR1(N598G)–NR2A, NR1–NR2A(N596G) and NR1(N598G)–NR2A(N596G) NMDA receptor channels

Subunit composition	X	ΔE_r (mV)	n	P_X/P_K
	K^+	0	—	1·0
NR1(N598G)–NR2A	MA	−10·4 ± 0·4	6	0·69
	DMEtOHA	−48·0 ± 0·6	6	0·15
	TMA	−71·8 ± 0·5	6	0·06
	TEA	−100·0 ± 1·2	5	0·016
NR1–NR2A(N596G)	MA	−9·5 ± 0·3	5	0·71
	DMEtOHA	−53·1 ± 1·1	6	0·12
	TMA	−84·7 ± 0·6	6	0·03
	TEA	< −115	4	—
NR1(N598G)–NR2A(N596G)	DMA	−14·7 ± 0·2	5	0·58
	DEA	−22·0 ± 0·2	4	0·43
	DMEtOHA	−33·6 ± 0·7	6	0·27
	TMA	−42·2 ± 0·3	5	0·19
	Tris*	−43·4 ± 0·5	7	0·18
	TEA	−70·3 ± 0·3	5	0·06
	TEA*	−71·7 ± 0·5	6	0·05

Reference solution (mM): 103·5 KCl, 10 Hepes, 0·18 $CaCl_2$; test solution (mM): 100 XCl, 10 histidine, 0·18 $CaCl_2$. *Test solutions (mM): 100 Tris, 10 Hepes, 0·18 $CaCl_2$ or 103·5 mM TEACl, 10 Hepes, 0·18 $CaCl_2$. Permeability ratios were calculated using eqn (3). Values of ΔE_r are means ± S.E.M.

asparagine was replaced by the positively charged and bulkier arginine the permeability of DMA was greatly increased. In contrast to the strong effects of mutations at the N-site, mutation of the N + 1 serine or the N + 2 glycine to smaller or larger sized amino acids did not produce significant changes in organic cation permeability. Hence, for the NR1-subunit, the asparagine occupying the N-site appears to contribute to the narrow constriction whereas the two amino acids upstream do not.

In contrast to the NR1 N-site, mutation of the NR2A N-site asparagine to smaller or larger sized amino acids had only small effects on organic cation permeability. Furthermore, as summarized in Fig. 6 (lower panel) and Table 5, mutation of the NR2A N-site asparagine to the larger glutamine, smaller serine or negatively charged aspartate changed the DMA permeability more than that for DEA, which we interpret as affecting binding rather than pore size. In addition, replacing the N-site asparagine with arginine decreased the DMA permeability. It was only when this asparagine was changed to glycine that a small effect on pore size occurred. However, much stronger effects were found when the asparagine residue occupying the N + 1 site was mutated. Indeed, mutation of the N + 1 site asparagine to the smaller serine or glycine or to the larger glutamine produced a volume-specific effect on organic cation permeability. In addition, mutation of the N + 2 site serine to glycine also produced a larger increase in the DEA permeability than that for DMA. Hence, for the NR2A-subunit, the N + 1 site asparagine and to a lesser extent the N + 2 site serine appear to contribute to the narrow constriction.

The double-mutant channel, NR1(N598G)–NR2A (N596G), has stronger effects on increasing the pore size than each individual mutant channel

Substituting the smaller glycine for the asparagine at the NR1 N-site or the NR2A N + 1 site strongly increased organic cation permeability. To test if other structural elements contribute to the narrow constriction, we quantified the size of the narrow region for wild-type channels, for the two individual mutant channels, NR1(N598G)–NR2A and NR1–NR2A(N596G), as well as for the double-mutant channel, NR1(N598G)–NR2A (N596G). This required measuring the permeability of a wide range of differently sized organic cations (Table 6). Figure 7 depicts current records for the double-mutant channel. The shift in the reversal potential on replacing external K^+ with DMA (Fig. 7*A*) or DEA (Fig. 7*B*) was nearly 25 and 40 mV less negative, respectively, than that of wild-type channels and gave ratios P_{DMA}/P_K of 0·58 ($n = 5$) and P_{DEA}/P_K of 0·43 ($n = 4$), values considerably larger than those of the wild-type as well as each individual mutant channel. This large increase in DMA and DEA permeability suggests a greatly increased pore size, and the buffer histidine may also permeate. Therefore histidine was not included in solutions to test the larger organic cations Tris and TEA (see Methods), which are impermeant in wild-type channels (Villarroel *et al.* 1995). On replacing external K^+ with Tris (Fig. 7*C*) or TEA

(Fig. 7*D*), the shift in the reversal potential was −42·5 and −71·5 mV, respectively, giving ratios P_{Tris}/P_K of 0·18 ($n = 7$) and P_{TEA}/P_K of 0·05 ($n = 6$). Also, P_{TEA}/P_K measured in a solution containing histidine showed a slightly larger value ($P_{TEA}/P_K = 0{\cdot}06$; Table 6) suggesting that histidine may permeate but that the contribution of histidine permeation to the permeability measured for the more highly permeant organic cations would be insignificant.

We also considered the the possibility that the double-mutant channel may be permeable to anions. However, the shift in the reversal potential on replacing 103·5 mM K^+ with the same solution diluted by one-half was indistinguishable for wild-type (−17·2 ± 0·5 mV, $n = 3$) and mutant (−17·1 ± 0·6 mV, $n = 3$) channels and was similar to that predicted by a K^+-selective electrode (−17·6 mV).

To quantify the size of the narrow constriction, we plotted the permeability of the test cation as a function of the cross-sectional area of its two smallest dimensions and fitted a linear equation to these plots (Fig. 8). We defined the limiting size of the narrow constriction as the intercept at a permeability of 0·01. With this definition, the wild-type channel constriction had a surface area of 0·24 nm^2 and a calculated cross-sectional diameter of 0·55 nm, in good agreement with earlier reports (Villarroel *et al.* 1995; Zarei & Dani, 1995). For the NR2(N596G) mutant channels, the narrow constriction was increased to 0·67 nm whereas the NR1(N598G) mutation increased it slightly more to 0·75 nm. The narrow constriction of the double-mutant channel was increased to 0·87 nm, which is the sum of the increase observed for the two individual mutant channels.

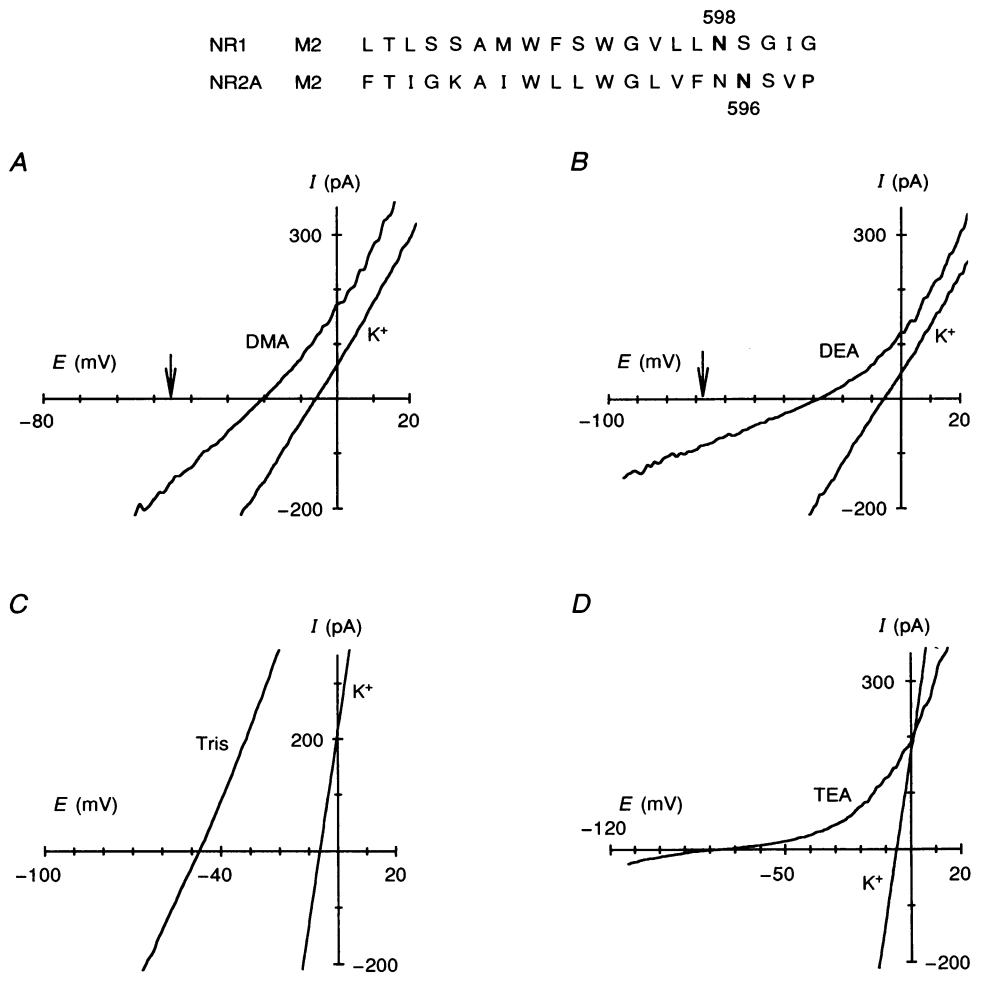

Figure 7. The double mutation, NR1(N598G)–NR2A(N596G), shifts the reversal potential of organic cations in a positive direction more than the individual mutations

Glutamate-activated currents were recorded and displayed as in Fig. 1 except that macropatches were isolated from oocytes expressing the double-mutant channel, NR1(N598G)–NR2A(N596G). In *C* and *D* no arrows are shown since these organic cations are impermeant in wild-type channels. The Tris and TEA solutions were buffered using Hepes. The amino acid sequences of the wild-type NR1- and NR2A-subunit M2 domains are shown at the top (see Fig. 2).

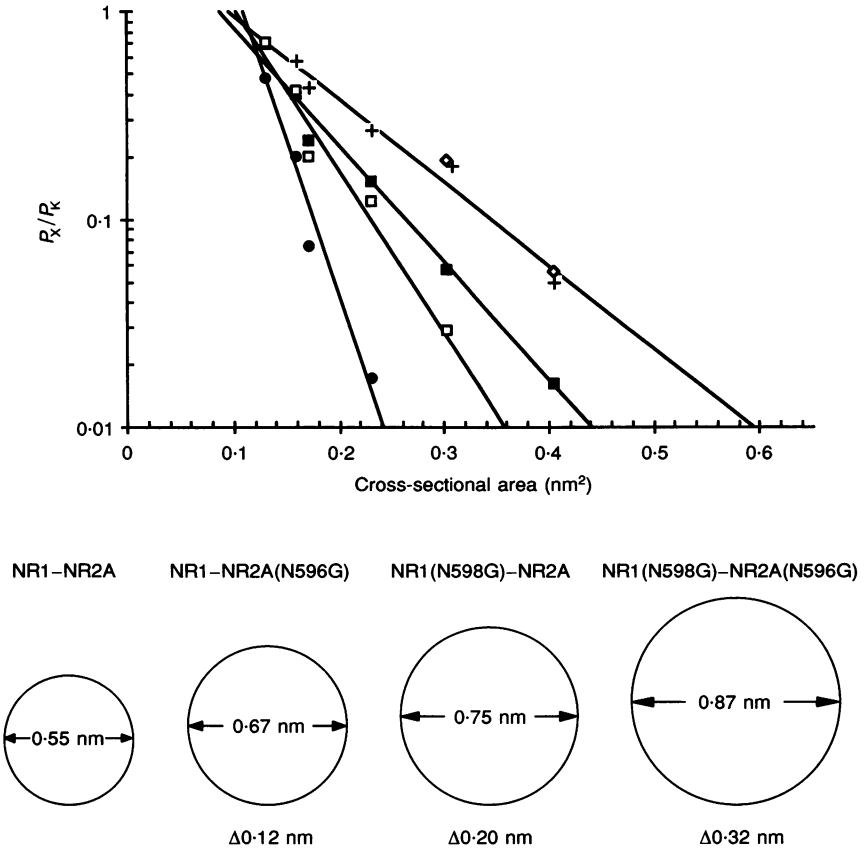

Figure 8. The double-mutant channels, NR1(N598G)–NR2A(N596G), have a narrow constriction which is larger than those of each individual mutant channel

The organic cation permeability for wild-type (●), NR1–NR2A(N596G) (□), NR1(N598G)–NR2A (■), and NR1(N598G)–NR2A(N596G) (+) channels are plotted as a function of the cross-sectional area of the two smallest dimensions of the organic cation (see Table 2). ◇ in the NR1(N598G)–NR2A(N596G) plot are the permeability measurements for TMA and TEA using solutions containing histidine as a buffer, but were not included in the fit.

DISCUSSION

Native NMDA receptor channels are heteromultimers composed of NR1- and NR2-subunits with their M2 domains forming at least part of the permeation pathway. To identify the structural elements that contribute to the selectivity filter of the NMDA receptor channel, we mutated the N-site and two adjacent residues in the M2 domain of the NR1- and NR2A-subunits and found that amino acids in both subunits contribute to the narrow constriction but in a differing manner. Based on sequence alignment the two N-sites are homologous, yet the asparagine at the N-site of the NR1-subunit forms part of the selectivity filter, whereas for the NR2A-subunit the two amino acids adjacent to the N-site appear to have the same function.

Measurement of the size of the narrow constriction

We used the relative ease by which organic cations permeate wild-type and mutant NMDA receptor channels as an indicator of the size of the narrow constriction. An assumption of this approach is that the major determinant of the permeability of an organic cation is its size rather than its chemical nature (Dwyer *et al.* 1980; Hille, 1992). Consistent with this assumption, we found for wild-type as well as mutant NMDA receptor channels (Fig. 8) a linear relationship between the permeability of organic cations and the cross-sectional area of their two smallest dimensions despite the variable nature of the organic cations tested (see also Villarroel *et al.* 1995).

We screened most mutations for their effect on the permeability of DMA and the larger DEA and found that mutations with a permeability different from that of wild-type channels either produced a stronger relative effect on changing the permeability of DEA than that of DMA or vice versa. These two patterns are exemplified by the asparagine to glutamine mutations in the N-site of the two subunits (Fig. 3). For the NR1-subunit, this mutation produced only a small increase in the DMA permeability (1·2 times greater than wild type), but much stronger relative effects on the DEA (2·3 times greater) and

DMEtOHA (4·5 times greater) permeabilities. We interpreted this pattern, which was consistently seen for the NR1 N-site and NR2A N + 1 site mutations (Fig. 6), as reflecting a change in the size of the narrow constriction; if an organic cation is considerably smaller than the narrow constriction and assuming single-file movement of ions, it would be less sensitive to changes in the size of this region whereas larger sized organic cations would be more sensitive. On the other hand, for the NR2A-subunit, mutation of the N-site asparagine to glutamine significantly changed the permeability of only the smaller organic cations MA and DMA with no significant effect on the larger organic cations DEA and DMEtOHA. This pattern which occurred mainly with mutations at the NR2A N-site appears inconsistent with a change in pore size and may indicate that the mutations affect the affinity of the organic cation for the permeation pathway. Indeed, although all the organic cations carry a positive charge, the charge to surface area ratio decreases with increasing size of the organic cation and for smaller sized organic cations, this charge would contribute more to its permeability properties. For those mutations that apparently changed the pore size, a similar change in the affinity of organic cations for the permeation pathway cannot be excluded and seems likely to occur, given that mutations at the NR1 N-site, for example, also have strong effects on Ca^{2+} permeability (Burnashev *et al.* 1992; Table 1). Nevertheless, since this secondary permeation property of organic cations is relatively small and does not occur for larger sized organic cations, it would not significantly change the conclusions.

Both NR1- and NR2A-subunits contribute to the narrow constriction

Mutation of an asparagine at the N-site in the NR1-subunit or at the N + 1 site in the NR2A-subunit (Fig. 6) consistently changed the permeability of organic cations in a manner reflecting a change in pore size. Mutant channels containing the asparagine to glycine mutation at either position showed large increases in pore size based on the permeability of a wide range of differently sized organic cations (Fig. 8). In addition, the pore size of the double-mutant channel, NR1(N598G)–NR2A(N596G), increased to approximately the sum of that observed for the two individual mutant channels. Hence, the N-site asparagine in the NR1-subunit and the N + 1 site asparagine in the NR2A-subunit, which are not homologous based on sequence alignment, appear to be the major structural determinants of the selectivity filter. The NR1 N-site and NR2A N + 1 site asparagines appear not to contribute equally to this structure.

Quantitatively, the increase in the pore size for the double mutant was the sum of that produced by the individual mutants. However, for the double-mutant channel, the estimated size of the narrow constriction should be considered a reasonable approximation since only a limited range of organic cations was tested and no attempt was made to identify an impermeant organic cation. In addition, the P_{Ca}/P_K value measured for this channel may be overestimated since NMDG could also be permeant, but, since only 0·18 mM Ca^{2+} was present externally, a small error in P_{Ca} would not significantly change the calculated permeability ratios.

For the NR2A-subunit, replacement of the N + 1 site asparagine produced volume-specific effects on pore size (Fig. 6): the smaller glycine increased the narrow constriction from 0·55 nm for wild-type channels to approximately 0·67 nm, the similarly sized aspartate was without effect and the larger glutamine decreased the narrow constriction to approximately 0·48 nm. Hence, the volume of the side chain at this position appears to be an important structural determinant of the narrow constriction and this residue is positioned in the narrow constriction such that it can accommodate a bulkier side chain. On the other hand, mutations of the N-site asparagine in the NR1-subunit did not produce volume-specific effects on pore size since replacing it with the smaller glycine or larger glutamine both increased the pore size. The increase in pore size produced by the NR1(N598Q)–NR2A mutant channels is contrary to what is expected based on the volume of the side chain. Nevertheless, the narrow constriction of wild-type NR1–NR2A channels (0·55 nm; Villarroel *et al.* 1995; this study) is smaller than that of other ligand-gated channels, such as the nicotinic acetylcholine receptor channel (~0·70–0·74 nm; Dwyer *et al.* 1980; Wang & Imoto, 1992) and may not accommodate bulkier side chains. With this interpretation, the difference between the asparagines at the NR1 N-site and the NR2A N + 1 site, when replaced by larger side chains, may indicate that the side chain of the NR1 N-site points directly into the pore constriction whereas for the N + 1 site it is positioned at an angle. Indeed, for the NR1 N-site the native asparagine appears to be positioned tightly since replacing it with the smaller serine was without effect on pore size despite having the strongest effect of any mutation on reducing Ca^{2+} permeability (Table 1).

Alternatively, the opposite change in pore size when a larger side chain replaced the asparagines at the NR1 N-site or the NR2A N + 1 site could reflect a difference in subunit stoichiometry. For example, if the NMDA receptor channel is composed of five subunits, three of which are NR1-subunits, then the narrow constriction may not be able to accommodate the three bulkier glutamines in the NR1(N598Q)–NR2A mutant channels, but could accommodate the two glutamines in the NR1–NR2A(N596Q) mutant channels. However, this alternative seems unlikely since substituting serine for the NR1 N-site asparagine did not produce a change in pore size, whereas the same NR2A N + 1 site substitution did produce a strong increase.

It should also be noted that the lack of a volume-specific effect of the replacement of residues contributing to the narrow constriction of glutamate receptor channels is not unreasonable. If the M2 domain of glutamate receptor channels was a membrane-spanning

α-helix then it seems likely that a volume-specific effect would occur. However, there is growing evidence that the M2 domain in glutamate receptors forms a loop (Hollmann *et al.* 1994; Bennett & Dingledine, 1995; Wood, VanDongen & VanDongen, 1995), indicating that at least part of its secondary structure is not in an α-helical arrangement.

Although the side chains of the NR1 N-site and the NR2A N + 1 site appear to be the major structural elements that form the selectivity filter, it is unclear as to whether both point into the channel lumen. Mutation at either site tended to have strong effects on Ca^{2+} permeability (Table 1). However, in cysteine substitution mutants, the NR1 N-site is accessible to external methanethiolsulfonate ethylammonium (MTSEA), consistent with it pointing into the lumen, whereas the NR2A N + 1 site is not (Kuner, Seeburg & Sakmann, 1994). There appear to be two possible explanations: the N + 1 asparagine may be positioned on the internal face of the narrow constriction and may not be reached by external MTSEA. Alternatively, it may act as a scaffold upon which other amino acids rest. If the latter is true, the NR2A N + 2 site serine is a good candidate for pointing into the narrow constriction since it is accessible to external MTSEA and replacement of this residue with the smaller glycine strongly increased the pore size (Fig. 6). Furthermore, replacing it with a bulkier side chain (asparagine) increased the pore size in contrast to what is expected, suggesting that, like the NR1(N598Q) mutation, a bulkier side chain at this position may disrupt the narrow constriction.

The N-site asparagines are positioned asymmetrically

Based on sequence alignment, the N-site asparagines for the NR1- and NR2-subunits are located at homologous positions. Nevertheless, substitution of the two asparagines in the different subunits produced different patterns of changes in organic cation permeability suggesting that they are not positioned identically with respect to the vertical axis of the channel (Fig. 6). For the NR1-subunit, mutation of the N-site consistently produced a stronger relative effect on the permeability of DEA than that of DMA and the arginine mutation increased the permeability of DMA. In contrast, NR2A N-site mutations tended to produce stronger relative effects on the permeability of DMA than of DEA and the arginine mutation decreased the permeability of DMA. Despite these differences, the two N-sites are presumably positioned near each other since for the NR2A-subunit the adjacent asparagine at the N + 1 site contributes to the selectivity filter. In addition, replacement of the N-site asparagine by glycine in the NR2A-subunit also increased the pore size, albeit very weakly, suggesting that it is positioned near the selectivity filter. Hence, while the NR1 N-site asparagine contributes to the narrow constriction, the NR2A N-site asparagine lies adjacent to this region. Because mutation of the NR2A N-site asparagine produces strong effects on external Mg^{2+} block (Burnashev *et al.* 1992), it may be positioned on the external face of the selectivity filter, although additional experiments will be required to define precisely its position relative to the selectivity filter as well as the NR1 N-site asparagine.

Conclusion

The narrow constriction of the NMDA receptor channel is formed by amino acid residues in the M2 domain from both the NR1- and NR2A-subunits but these residues are not at homologous positions as predicted by sequence alignment. In addition, the contribution of the two subunits to the selectivity filter appears to be unequal. The asparagines at the NR1 N-site and the NR2A N + 1 site apparently point at an angle relative to each other.

Almers, W. & McCleskey, E. W. (1984). Non-selective conductance in calcium channels of frog muscle: calcium selectivity in a single-file pore. *Journal of Physiology* **353**, 585–608.

Ausubel, F. M., Brent, R., Kingston, R. E., Moore, D. D., Seidman, J. G., Smith, J. A. & Struhl, K. (1994). Mutagenesis of cloned DNA. In *Current Protocols in Molecular Biology*, vol. 1, chap. 8. John Wiley & Sons.

Bennett, J. A. & Dingledine, R. (1995). Topology profile for a glutamate receptor: three transmembrane domains and a channel-lining reentrant membrane loop. *Neuron* **14**, 373–384.

Burnashev, N. (1993). Recombinant ionotropic glutamate receptors: functional distinction imparted by different subunits. *Cellular Physiology and Biochemistry* **3**, 318–331.

Burnashev, N., Schoepfer, R., Monyer, H., Ruppersberg, J. P., Günther, W., Seeburg, P. H. & Sakmann, B. (1992). Control by asparagine residues of calcium permeability and magnesium blockade in the NMDA receptor. *Science* **257**, 1415–1419.

Chalfie, M., Tu, Y., Euskichen, G., Ward, W. W. & Prasher, D. C. (1994). Green fluorescent protein as a marker for gene expression. *Science* **263**, 802–805.

Choi, D. W. (1988). Glutamate neurotoxicity and diseases of the nervous system. *Neuron* **1**, 623–634.

Colquhoun, D., Jonas, P. & Sakmann, B. (1992). Action of brief pulses of glutamate on AMPA/kainate receptors in patches from different neurones of rat hippocampal slices. *Journal of Physiology* **458**, 261–287.

Cotman, C. W. & Monaghan, D. T. (1988). Excitatory amino acid neurotransmission: NMDA receptors and Hebb-type synaptic plasticity. *Annual Review of Neuroscience* **11**, 61–80.

Dwyer, T. M., Adams, D. J. & Hille, B. (1980). The permeability of the endplate channel to organic cations in frog muscle. *Journal of General Physiology* **75**, 469–492.

Gasic, G. P. & Hollmann, M. (1992). Molecular neurobiology of glutamate receptors. *Annual Review of Physiology* **54**, 507–536.

Hamill, O. P., Marty, A., Neher, E., Sakmann, B. & Sigworth, F. J. (1981). Improved patch-clamp technique for high resolution current recording from cells and cell-free membrane patches. *Pflügers Archiv* **391**, 85–100.

Hess, P. & Tsien, R. W. (1984). Mechanism of ion permeation through calcium channels. *Nature* **309**, 453–456.

Hille, B. (1992). *Ionic Channels of Excitable Membranes*, 2nd edn. Sinauer Associates, Inc., Sunderland, MA, USA.

HOLLMANN, M. & HEINEMANN, S. (1994). Cloned glutamate receptors. *Annual Review of Neuroscience* **17**, 31–108.

HOLLMANN, M., MARON, C. & HEINEMANN, S. (1994). N-glycosylation site tagging suggests a three transmembrane domain topology for the glutamate receptor GluR1. *Neuron* **13**, 1331–1343.

HOLLMANN, M., O'SHEA, G. A., ROGERS, S. W. & HEINEMANN, S. (1989). Cloning by functional expression of a member of the glutamate receptor family. *Nature* **342**, 643–648.

IKEDA, K., NAGASAWA, H., MORI, H., ARAKI, K., SAKIMURA, K., WATANABE, M., INOUE, Y. & MISHINA, M. (1992). Cloning and expression of the ϵ4 subunit of the NMDA receptor channel. *FEBS Letters* **313**, 34–38.

KUNER, T., SEEBURG, P. H. & SAKMANN, B. (1994). Cysteine-substitutions reveal structural asymmetry of the ion pore in NMDA receptor channels. *Society for Neuroscience Abstracts* **20**, 740.

KUTSUWADA, T., KASHIWABUCHI, N., MORI, H., SAKIMURA, K., KUSHIYA, E., ARAKI, K., MEGURO, H., MASAKI, H., KUMANISHI, T., ARAKAWA, M. & MISHINA, M. (1992). Molecular diversity of the NMDA receptor channel. *Nature* **358**, 36–41.

LESTER, H. A. (1992). The permeation pathway of neurotransmitter-gated ion channels. *Annual Review of Biophysics and Biomolecular Structure* **21**, 267–292.

LEWIS, C. A. (1979). Ion-concentration dependence of the reversal potential and the single channel conductance of ion channels at the frog neuromuscular junction. *Journal of Physiology* **286**, 417–445.

MACDERMOTT, A. B., MAYER, M. L., WESTBROOK, G. L., SMITH, S. J. & BARKER, J. L. (1986). NMDA receptor activation increases cytoplasmic calcium concentration in cultured spinal cord neurones. *Nature* **321**, 261–263.

MAYER, M. L. & MILLER, R. J. (1988). Excitatory amino acid receptors, second messengers and regulation of intracellular Ca^{2+} in mammalian neurons. *Trends in Pharmacological Sciences* **11**, 254–260.

MAYER, M. S., WESTBROOK, G. L. & GUTHRIE, P. B. (1984). Voltage-dependent block by Mg^{2+} of NMDA responses in spinal cord neurones. *Nature* **309**, 261–263.

MELDRUM, B. & GARTHWAITE, J. (1990). Excitatory amino acid neurotoxicity and neurodegenerative disease. *Trends in Pharmacological Sciences* **11**, 379–387.

METHFESSEL, C., WITZEMANN, V., TAKAHASHI, T., MISHINA, M., NUMA, S. & SAKMANN, B. (1986). Patch clamp measurements on *Xenopus laevis* oocytes: currents through endogenous channels and implanted acetylcholine receptor and sodium channels. *Pflügers Archiv* **407**, 577–588.

MONYER, H., SPRENGEL, R., SCHOEPFER, R., HERB, A., HIGUCHI, M., LOMELI, H., BURNASHEV, N., SAKMANN, B. & SEEBURG, P. H. (1992). Heteromeric NMDA receptors: molecular and functional distinction of subtypes. *Science* **256**, 1217–1221.

MORIYOSHI, K., MASU, M., ISHII, T., SHIGEMOTO, R., MIZUNO, N. & NAKANISHI, N. (1991). Molecular cloning and characterization of the rat NMDA receptor. *Nature* **354**, 31–37.

NOWAK, L., BREGESTOVSKY, P., ASCHER, P., HERBET, A. & PROCHIANTZ, A. (1984). Magnesium gates glutamate-activated channels in mouse central neurones. *Nature* **307**, 462–465.

RADITSCH, M., RUPPERSBERG, J. P., KUNER, T., GUNTHER, W., SCHOEPFER, R., SEEBURG, P. H., JAHN, W. & WITZEMANN, V. (1993). Subunit-specific block of cloned NMDA receptors by argiotoxin$_{636}$. *FEBS Letters* **324**, 63–66.

SCHALL, T. J., LEWIS, M., KOLLER, K. J., LEE, A., RICE, G. C., WONG, G. H. W., GATANAGA, T., GRANGER, G. A., LENTZ, R., RAAB, H., KOHR, W. J. & GOEDDEL, D. V. (1990). Molecular cloning and expression of a receptor for human necrosis factor. *Cell* **61**, 361–370.

SHENG, M., CUMMINGS, J., ROLDAN, L. A., JAN, Y. N. & JAN, L. Y. (1994). Changing subunit composition of heteromeric NMDA receptors during development of rat cortex. *Nature* **368**, 144–147.

SUGIHARA, H., MORIYOSHI, K., ISHII, T., MASU, M. & NAKANISHI, S. (1992). Structures and properties of seven isoforms of the NMDA receptor generated by alternative splicing. *Biochemical and Biophysical Research Communications* **185**, 826–832.

TSUZUKI, K., MOCHIZUKI, S., IINO, M., MORI, H., MISHINA, M. & OZAWA, S. (1994). Ion permeation properties of the cloned mouse epsilon 2/zeta 1 NMDA receptor channel. *Molecular Brain Research* **26**, 37–46.

VILLARROEL, A., BURNASHEV, N. & SAKMANN, B. (1995). Dimensions of the narrow portion of a recombinant NMDA receptor channel. *Biophysical Journal* **68**, 866–875.

WANG, F. & IMOTO, K. (1992). Pore size and negative charge as structural determinants of permeability in the Torpedo nicotinic acetylcholine receptor channel. *Proceedings of the Royal Society* B **250**, 11–17.

WO, Z. G. & OSWALD, R. E. (1995). Unraveling the modular design of glutamate-gated ion channels. *Trends in Neurosciences* **18**, 161–168.

WOOD, M. W., VANDONGEN, H. M. A. & VANDONGEN, A. M. J. (1995). Structural conservation of ion conduction pathways in K channels and glutamate receptors. *Proceedings of the National Academy of Sciences of the USA* **92**, 4882–4886.

ZAREI, M. M. & DANI, J. A. (1994). Ionic permeability characteristics of the *N*-methyl-D-aspartate receptor channel. *Journal of General Physiology* **103**, 231–248.

ZAREI, M. M. & DANI, J. A. (1995). Structural basis for explaining open-channel blockade of the NMDA receptor. *Journal of Neuroscience* **15**, 1446–1454.

Acknowledgements

We thank Drs G. Borst and A. Villarroel for their comments on the manuscript, M. Kaiser, S. Grünewald, A. Herold and Dr G. Köhr for technical help and advice, and Dr R. Schoepfer for initial support. This work was supported in part by Sonderforschungsbereich (SFB) Grant 317/B9 (P.H.S.) and a Long-term Human Frontier Science Fellowship (L.P.W.).

Received 3 August 1995; accepted 17 October 1995.